J. Fluid Mech. (2006), *vol.* 558, *pp.* 33–52.
doi:10.1017/S0022112006009839 Printed in the United Kingdom

An experimental investigation of the stability of the circular hydraulic jump

By JOHN W. M. BUSH[1], JEFFREY M. ARISTOFF[1] AND A. E. HOSOI[2]

[1]Department of Mathematics, Massachusetts Institute of Technology, 77 Massachusetts Avenue, Cambridge, MA 02139, USA

[2]Department of Mechanical Engineering, Massachusetts Institute of Technology, 77 Massachusetts Avenue, Cambridge, MA 02139, USA

(Received 3 March 2003 and in revised form 14 November 2005)

We present the results of an experimental investigation of the striking flow structures that may arise when a vertical jet of fluid impinges on a thin fluid layer overlying a horizontal boundary. Ellegaard *et al.* (*Nature*, vol. 392, 1998, p. 767; *Nonlinearity*, vol. 12, 1999, p. 1) demonstrated that the axial symmetry of the circular hydraulic jump may be broken, resulting in steady polygonal jumps. In addition to these polygonal forms, our experiments reveal a new class of steady asymmetric jump forms that include structures resembling cat's eyes, three- and four-leaf clovers, bowties and butterflies. An extensive parameter study reveals the dependence of the jump structure on the governing dimensionless groups. The symmetry-breaking responsible for the asymmetric jumps is interpreted as resulting from a capillary instability of the circular jump. For all steady non-axisymmetric forms observed, the wavelength of instability of the jump is related to the surface tension, σ, fluid density ρ and speed U_v of the radial outflow at the jump through $\lambda = (74 \pm 7)\sigma/(\rho U_v^2)$.

1. Introduction

The circular hydraulic jump may arise when a fluid jet falling vertically at high Reynolds number strikes a horizontal plate. Fluid is expelled radially, and the layer generally thins until reaching a critical radius at which the layer depth increases abruptly (figure 1). Predictions for the jump radius based on inviscid theory were presented by Rayleigh (1914). The dominant influence of fluid viscosity on the jump radius was elucidated by Watson (1964), who developed an appropriate description of the boundary layer on the impact plate. Subsequent theoretical studies of the circular jump have focused principally on describing the boundary layer separation and the associated dynamic pressure distribution behind the jump (Bowles & Smith 1992; Bohr, Dimon & Putkaradze 1993; Bohr, Putkaradze & Watanabe 1997; Higuera 1994, 1997; Ellegaard *et al.* 1996; Yokoi & Xiao 2000, 2002; Watanabe, Putkaradze & Bohr 2003). While substantial progress has been made, the complexity of this free-surface flow problem has precluded the development of a complete understanding of the problem. A review of studies of the circular hydraulic jump is presented by Bush & Aristoff (2003), who elucidate the influence of surface tension on its radius.

Both Craik *et al.* (1981) and Liu & Lienhard (1993) noted asymmetric instabilities in circular hydraulic jumps, and suggested the importance of surface tension in the frontal instability; however, no mechanism for instability was proposed. Moreover, as their working fluid was water, the resulting asymmetric jumps were irregular and

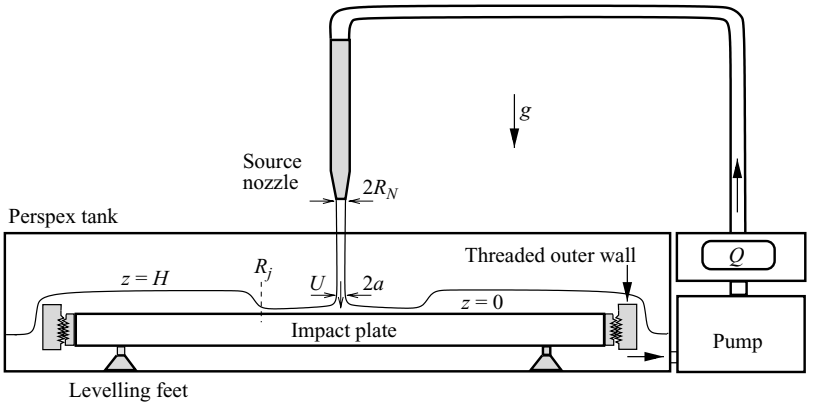

FIGURE 1. A schematic illustration of the experimental apparatus. Fluids were pumped through the source nozzle with a prescribed flux Q. The outer depth H was controlled by an outer wall whose height was adjustable.

unsteady. Liu & Lienhard (1993) characterized the dependence of the resulting unsteady jump forms on the governing dimensionless groups. The observed dependence on the jump Weber number clearly indicated the significance of surface tension on the jump stability.

Ellegaard *et al.* (1998) identified that a striking instability may transform the circular hydraulic jump into steady regular polygons. Experiments were conducted with ethylene glycol and a source nozzle of radius 0.5 cm at elevations of 1–5 cm above the lower boundary ejecting fluxes between 30 and 50 ml s^{-1}. The dependence of the jump planform on the nozzle height and flux rate was reported by Ellegaard *et al.* (1999); however, the dependence of the flow structure on the governing parameters was not fully elucidated. While a suggestion was made that the jump forms could be understood if an effective line tension was ascribed to the jump, no clear mechanistic explanation of the instability was given. We here extend the experimental study of these authors in order to gain further insight into the problem.

In § 2, we describe the experimental technique employed in our study, and in § 3 describe the variety of jump shapes observed in our exploration of parameter space. In § 4, we identify the dimensionless groups that govern the system, and detail the dependence of the jump form on these parameters. The dependence of the mean jump radius of the asymmetric forms is investigated in § 5. A scaling argument for the dependence of the wavelength of instability of the steady asymmetric jumps on the governing parameters is proposed in § 6.

2. Experimental technique

Figure 1 is a schematic illustration of our experimental apparatus. Fluids were pumped through the flowmeter and source nozzle, resulting in a falling jet that impacted the centre of a circular glass target plate of diameter 36 cm. The nozzle height was varied between 1 and 5 cm above the target plate. Beyond the hydraulic jump, the fluid ultimately spilled over the edges of the reservoir, and was recycled through the pump. The reservoir depth H was controlled by an adjustable outer wall and measured with a micrometer point gauge 3 cm from the outer edge of the reservoir. The asymmetric jump structures were extremely sensitive to any variations from horizontal; consequently, great care was taken in levelling the system in order to ensure that the

reservoir spilled uniformly over the bounding outer wall. The system was levelled to 1 part in 24 000 by adjusting its three support legs, and measuring the deflection from horizontal of the impact plate and reservoir rim with a Sterret level. The position of the jump was measured from radial gradations on the target plate surface.

The variable flow pump (Cole Parmer, Model 75225-00) was capable of fluxes in the range of 0–100 ml s^{-1} for the fluids examined in our study. The flow rate was measured with an AW Company Model JFC-01 digital flowmeter accurate to 0.1 % over the range considered. Viscosity measurements accurate to 0.14 % were made with Cannon-Fenske Routine tube viscometers. Fluid density was measured with an Anton-Parr 35N densitometer, accurate to 0.01 %. Surface tension measurements accurate to 0.1 dyn cm^{-1} were made with a Kruss K10 surface tensiometer. The bulk of the experiments were conducted with glycerol–water solutions with viscosities in the range 1–35 cS, densities 1.0–1.2 g cm^{-3} and surface tensions between 60 and 70 dyn cm^{-1}. We also used a pure mineral oil (Crystal Plus 70FG Oil, STE Oil Company Inc.), for which $\rho = 0.83$ g cm^{-3}, $\nu = 11$ cm^2 s^{-1} and $\sigma = 29.7$ dyn. Finally, we incorporate the data of Ellegaard *et al.* (1999), who used ethylene glycol for which $\rho = 1.1$ g cm^{-3}, $\nu = 11$ cm^2 s^{-1} and $\sigma = 47.7$ dyn cm^{-1}. Outer layer depths were varied from 0.2 to 1.5 cm.

Four nozzles were used, of radii 0.2, 0.38, 0.45 and 0.5 cm. The inner nozzle surfaces were smoothed and tapered near their exits in order to suppress turbulence and encourage laminar outflow in the parameter regime considered. While the details of the cross-sectional flow profiles were not measured, the nozzles were designed according to the specifications of McCarthy & Malloy (1974) with a narrow taper in order to flatten the profiles. Their suggestion is that the jet profiles will be relatively flat provided the taper angle lies between 45° and 70°. A recent study by Bergthorsson *et al.* (2005) demonstrates that the jet profiles will in general depend on the nozzle length, taper, and the jet Reynolds number and that, in certain ideal situations, the three may be varied in order to ensure a flat jet profile. While tuning these control parameters in order to ensure that the jet profiles are perfectly flat was not practical for our study, we worked from the assumption that the jet profiles are flat to leading order. A series of experiments was performed to test the sensitivity of the jump structure to the nozzle design. Turbulence generated in the nozzle by the addition of an obstacle was evident in the irregular, perturbed surface of the jet and that of the resulting jump. Two nozzles with identical outlet radii (0.32 cm) but different tapers (45° and 70°) were examined, and found to produce indistinguishable jump forms. Intervening taper angles were examined through addition of mylar sheets inside the nozzle with the sharper taper; over the range of Reynolds numbers and tapers considered, no qualitative changes in jump form were observed.

Flow speeds could be measured by tracking microbubbles introduced in the source fluid using a Redlake Motionscope Model PCI 8000S high-speed video camera. Adequate resolution of the bubbles typically required that we record at 500 frames per second with 0.001 s exposure times. The video footage was analysed using Midas Version 2.08 particle tracking software.

3. Observations

The variety of strictly circular jumps that may arise has been documented by Craik *et al.* (1981) and Liu & Lienhard (1993). Owing to its relevance to the jump stability, we recall here the transitions of the circular jump that arise as the outer depth is increased, from Type I to IIa and IIb jumps (see figure 2). We follow Ellegaard *et al.*

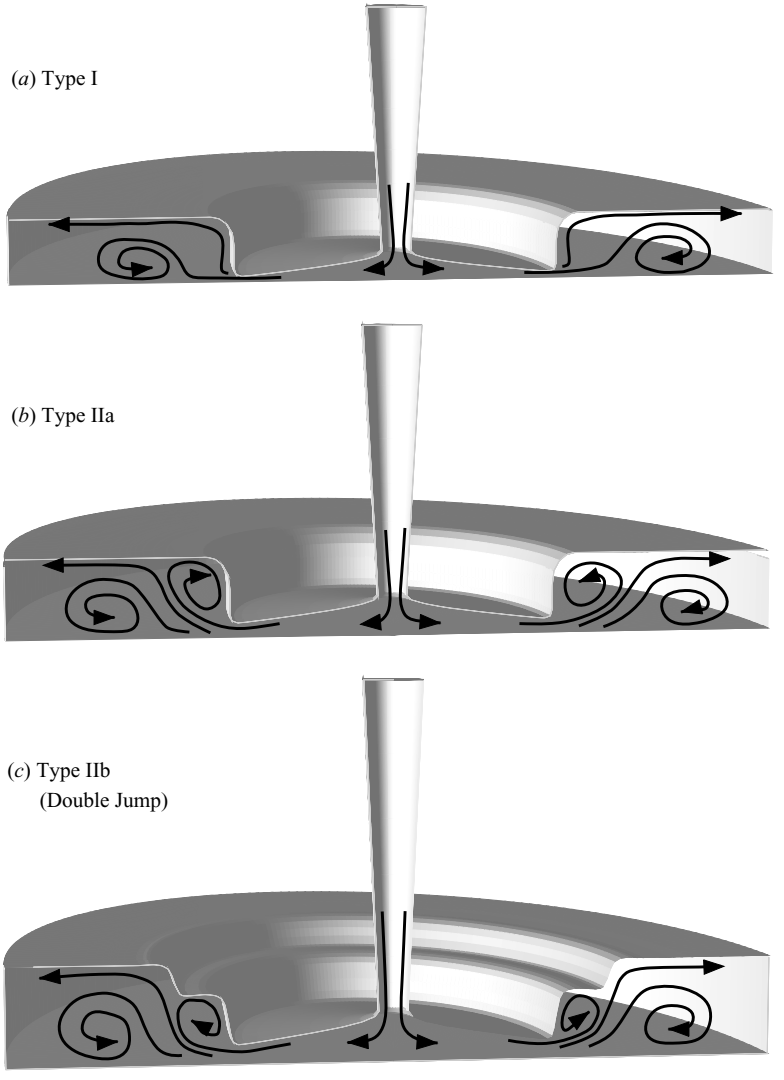

FIGURE 2. A schematic illustration of the progression in flow structure of the circular laminar hydraulic jump prompted by increasing the outer depth. The steady symmetry-breaking instabilities emerge exclusively from the Type II jumps.

(1996) in the Type I and II nomenclature, and Liu & Lienhard (1993) in distinguishing between Types IIa and IIb. The Type I jump is the standard circular hydraulic jump in which the surface flow is everywhere radially outward; the interior flow is radially outwards everywhere except within a recirculating region just downstream of the jump (Tani 1949). The Type IIa jump is similarly marked by a subsurface 'separation bubble', but also by a region of reversed surface flow adjoining the jump. As the outer depth increases further, the jump transforms into a Type IIb jump marked by a tiered or 'double-jump' structure. A key observation is that the axial symmetry-breaking instabilities reported by Ellegaard *et al.* (1998, 1999) and observed in our study occur exclusively for Type II jumps. At higher flow rates, the jumps become irregular and time-dependent, and may ultimately be marked by air entrainment at their base.

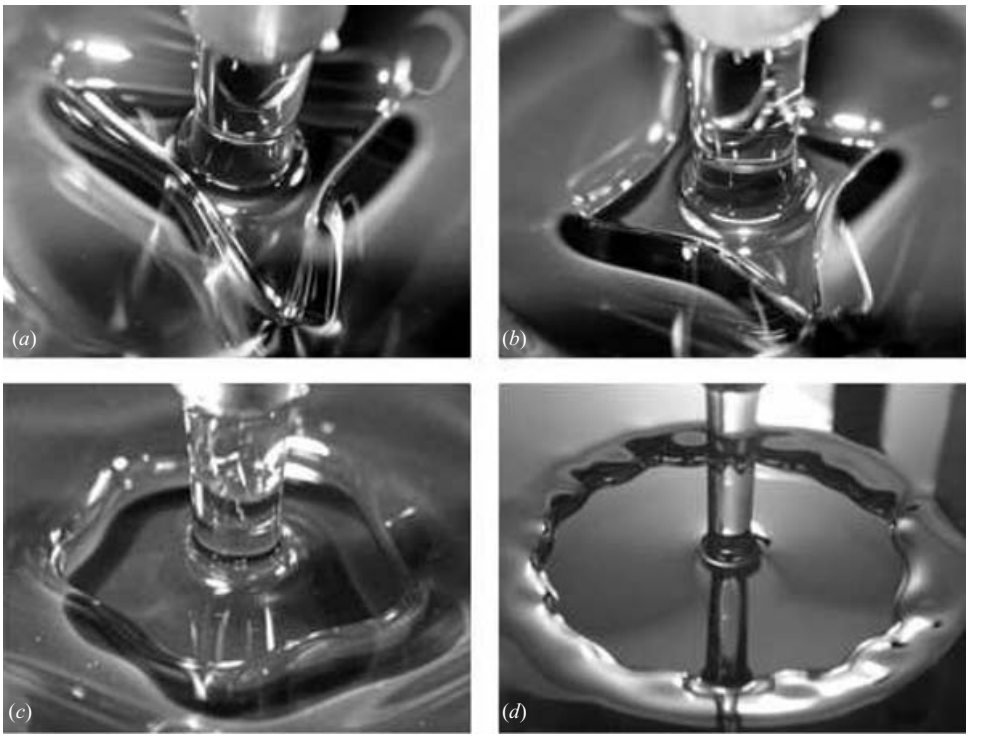

FIGURE 3. A number of jump shapes observed in the polygon regime: (*a*) triangle, (*b*) square, (*c*) pentagon, (*d*) *n*-gon.

At the highest flow rates examined, the flow within the thin film becomes turbulent (Watson 1964). We here restrict our attention to the case of laminar upstream flow in which there is no air entrainment at the jump.

The 0.5 cm nozzle radius corresponds to that used in the study of Ellegaard *et al.* (1998, 1999) and yielded the most regular polygonal jumps. Examples of the polygonal jump structures observed in our experiments are presented in figure 3. Varying the nozzle size and test fluid allowed us to explore a new regime marked by steady stable structures that included oval-, cat's eye-, bowtie-, butterfly- and clover-shaped jumps, henceforth all referred to as the 'clover regime'. Shapes arising in the clover regime are presented in figure 4. We note that the jumps arising in the clover regime are marked by the tiered structure characteristic of the Type IIb jumps. Some polygonal and clover forms were subject to weak time-dependent fluctuations, typically characterized by a net rotational motion of the entire jump structure, or the propagation of wave-like disturbances towards a single point on the jump.

The flow that accompanies the polygonal jumps is described by Ellegaard *et al.* (1999), and was visualized here through tracking microbubbles suspended in the flow. An example of bubble traces apparent in the corner region of a polygonal jump are illustrated in figure 5. The axial symmetry within the radially expanding film is evidently broken when the flow reaches the jump. Fluid is partially redirected along the jump front and so funnelled towards the corners of the jump, resulting in radial jets emerging from the corners. In the clover regime, the vortices adjoining the jump have a limited vertical extent, thus giving jumps in the clover regime their two-tiered structure (figure 2*c*).

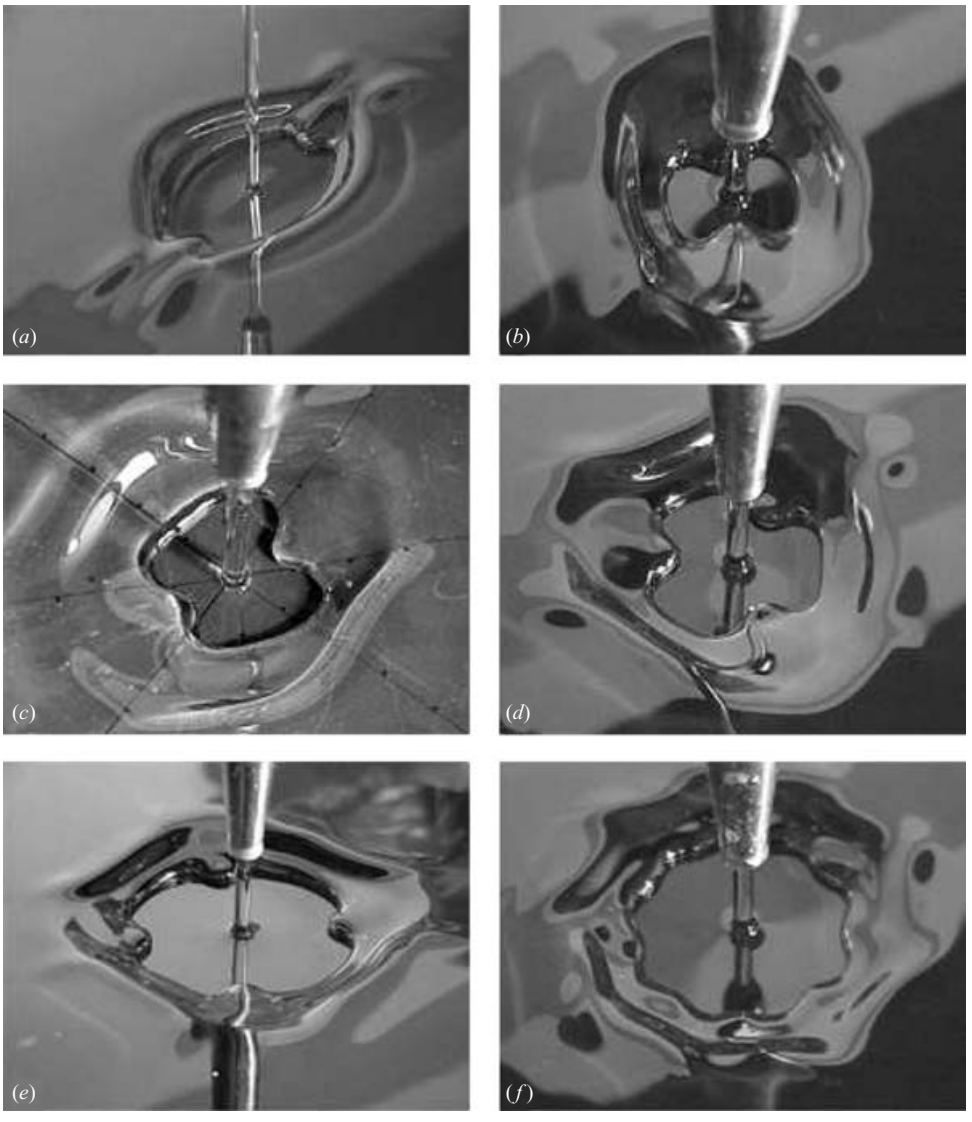

FIGURE 4. Jump shapes observed in the clover regime: (*a*) cat's eye, (*b*) bowtie, (*c*) butterfly, (*d*) three-leaf clover, (*e*) four-leaf clover, (*f*) octagonal clover. Note the tiered double-jump structure characteristic of the Type IIb regime.

The significance of surface tension for the frontal instability was clearly and simply demonstrated. The flow parameters were set in order to obtain a steady pentagonal jump of mean radius 2 cm. A small volume (1–2 drops) of surfactant (either a super-wetting agent or a commercial detergent) was added to the reservoir fluid, and resulted in the three qualitative changes apparent in figure 6. First, the jump expanded, with its mean radius increasing by approximately 20 %. Second, the polygonal instability was suppressed, and the jump assumed a circular form. Third, the jump became significantly less abrupt. The increase in mean radius is consistent with the theoretical predictions of Bush & Aristoff (2003) for the influence of the curvature force. The suppression of the polygonal form clearly indicates the importance of surface tension on the jump stability, the nature of which will be discussed in § 6.

FIGURE 5. A streak image illustrating bubble tracks in the neighbourhood of the corners of the hydraulic jump. The shutter speed was 1/100 s; the image thus illustrates clearly the high speed of the flows. Note the regions of recirculation adjoining the jump and the vigorous vortices adjoining the corners.

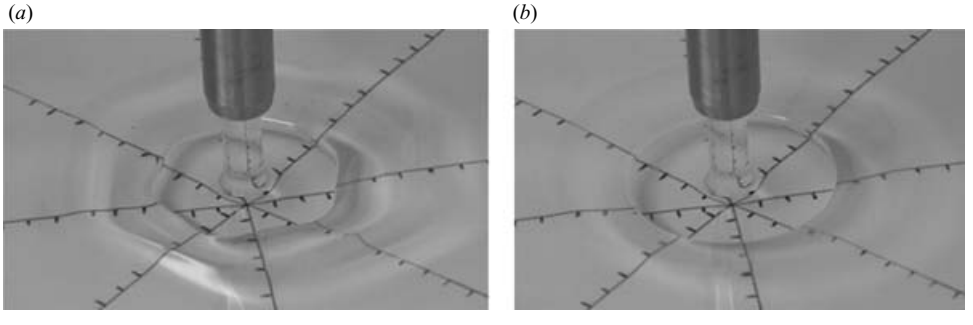

FIGURE 6. The influence of surfactant on the polygonal hydraulic jump. (*a*) A polygonal hydraulic jump generated with a glycerol–water solution. ($\rho = 1.1\,\mathrm{g\,cm^{-3}}$, $Q = 51\,\mathrm{cm^3\,s^{-1}}$, $H = 0.65\,\mathrm{cm}$, $\nu = 10\,\mathrm{cS}$, $a = 0.5\,\mathrm{cm}$). (*b*) The same configuration after the addition of a surfactant (liquid Dove) to the reservoir, which reduces the surface tension from 70 to $40\,\mathrm{dyn\,cm^{-1}}$. The addition of surfactant causes the polygonal jump to relax into a circular form, and to expand slightly. Radial gradations indicate intervals of 0.5 cm.

4. Parameter study

We consider a nozzle of radius R_N ejecting fluid downward at uniform speed U_0; the associated flux is $Q = \pi R_N^2 U_0$. The jet descends a distance Z in a gravitational field $-g\hat{z}$ before striking a rigid horizontal boundary covered by fluid of outer depth H (figure 1). The source conditions may be eliminated from consideration by

straightforward application of Bernoulli's equation. However, nozzle source conditions generally lead to variance from the predictions of inviscid theory (e.g. Bergthorsson *et al.* 2005); consequently, the jet radius at impact is measured with calipers. We further assume that the jet velocity profile at the point of impact is flat (independent of radius), and that the overlying air is not dynamically significant.

We thus consider a vertical jet of radius a and flux Q of fluid with viscosity ν and density ρ impacting a horizontal boundary covered by fluid of depth H at uniform speed $U = Q/(\pi a^2)$. The free surface is characterized by a constant surface tension σ. There are thus seven physical variables, a, H, Q, ν, ρ, g and σ expressible in terms of three fundamental units. Dimensional analysis indicates that the system may be uniquely prescribed by four dimensionless groups. We choose the jet Reynolds number $Re = Q/(\nu a)$, the jump Weber number $We = \rho Q^2/(\sigma H^3)$, the Bond number $B = \rho g a^2/\sigma$, and the relative magnitudes of the impacting jet radius and the outer layer depth, a/H. We proceed by elucidating the dependence of the form of the jump structure on these four governing dimensionless groups. We note that the commonly used Froude number is expressible in terms of the Bond and Weber numbers.

Two-dimensional projections of the four-dimensional parameter space are presented in figures 7 and 8. Each corresponds to a series of experiments represented by a plane in figure 9, and performed with a fixed nozzle radius and fluid, and so a constant B. Figure 7(a) illustrates the dependence of jump structure on Re and We for a source nozzle of radius 0.5 cm located a distance 2.5 cm above the impact plane ejecting a glycerol–water solution with viscosity $\nu = 10$ cS and density $\rho = 1.12\,\mathrm{g\,cm^{-3}}$. The corresponding Bond number is $B = 4.62$. Each diagonal trace indicates the influence of increasing flux Q at a fixed outer depth H. Critical H values for the transitions between the various flow forms are indicated. At the lowest H value examined, 0.45 cm, the jumps assume the circular Type I planform. When the layer depth is increased to $H = 0.57$ cm, the jumps assume the Type IIa planform, and so are marked by a recirculating vortex and reversed surface flow adjoining the jump. Further increasing H prompts the symmetry-breaking instability responsible for polygonal jumps (figure 3). Polygons with number of sides between 3 and 10 occupy well-defined regions of parameter space, with the larger number of sides being observed at higher flow rates and mean jump radii. We note that the transitions between different polygonal shapes occur at roughly constant Weber numbers. For $H > 0.83$ cm ($H/a > 4.13$), no jumps arise: the jet simply plunges into the reservoir, typically entraining air in the process. The corresponding projection of these data onto the (a/H, We)-plane is presented in figure 7(b).

Figure 8 illustrates an equivalent regime diagram describing a series of experiments conducted with a nozzle of radius 0.2 cm located at height 2.5 cm above the plane and ejecting a glycerine–water solution of viscosity 32 cS. As the outer layer depth increases progressively, the jump evolves from circular Type I to Type II forms, and then to an asymmetric form. In this parameter regime, the asymmetric forms are those arising in the clover regime (figure 4): cat's eyes, bowties, butterflies or clovers. At the largest H values examined, the jump is turbulent: air is entrained at the base of the jump, giving rise to irregular, unsteady motion such as that observed by Liu & Lienhard (1993) in water. The corresponding projection of these data onto the (a/H, We)-plane is presented in figure 8(b).

A series of three-dimensional regime diagrams illustrating the dependence of the jump structure on (Re, We, a/H) is presented in figure 9. Each regime diagram corresponds to a particular Bond number. For the glycerine–water solutions, whose densities and surface tensions varied by no more than 5 %, the constant Bond number

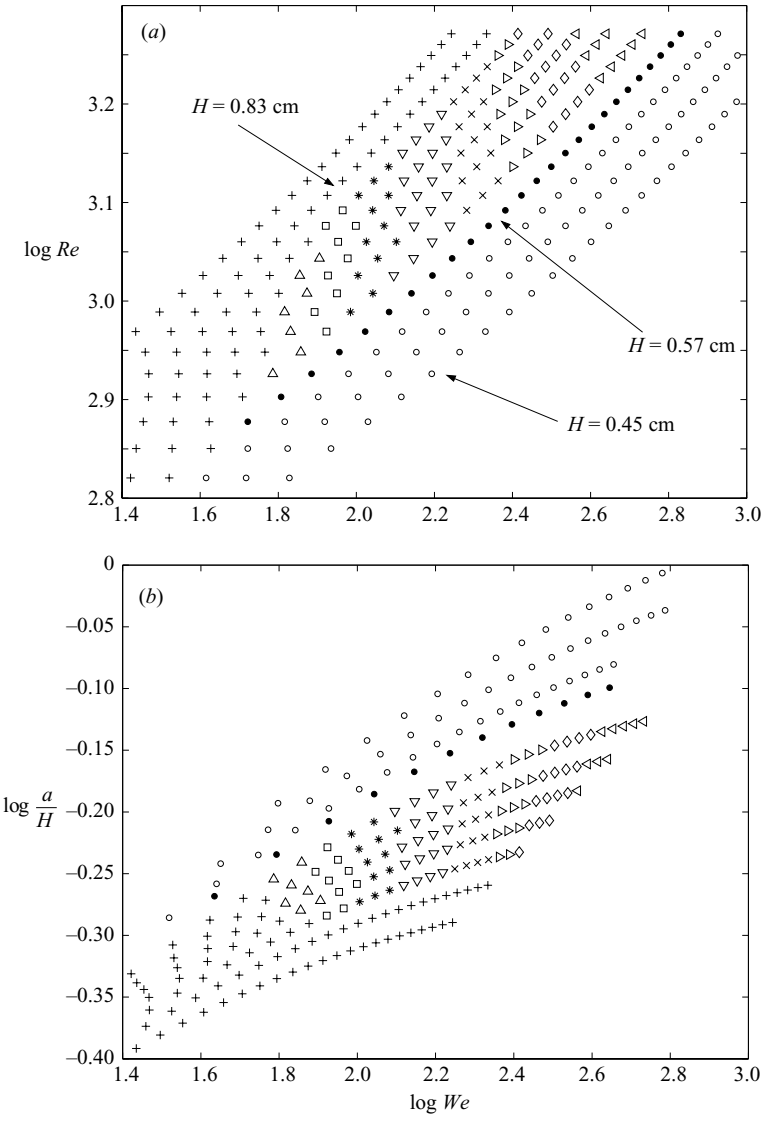

FIGURE 7. Two-dimensional projections of the surface of data obtained at $B = 4.62$ and presented in figure 9(*a*). All jumps were formed by a glycerine–water solution of viscosity 10 cS being released from a nozzle of radius 0.5 cm at a height 2.5 cm above the impact plate. (*a*) The dependence of the jump form on $Re = Qa/\nu$, and $We = \rho Q^2/(\sigma H^3)$. Different symbols denote the various jump shapes: △, three-sided; □, four-sided; ∗, five-sided; ▽, six-sided; ×, seven-sided; ▷, eight-sided; ◇, nine-sided; ◁, 10-sided; ○, Type I; ●, Type II; +, no jump. (*b*) The analogous dependence of jump structure on a/H and *We*.

corresponds to a fixed nozzle diameter. For the experiments conducted with mineral oil, nozzles were designed specifically to match B with either the glycerine-water experiments (figure 9*a*) or the experiments of Ellegaard *et al.* (1998, 1999) (figure 9*d*). The data fall onto distinct surfaces such as those whose two-dimensional projections are presented in figures 7 and 8, each corresponding to a different working fluid. For the sake of clarity, we classify jumps as being either Type I, II, polygons, clovers or turbulent, and do not distinguish between the various types of polygonal and

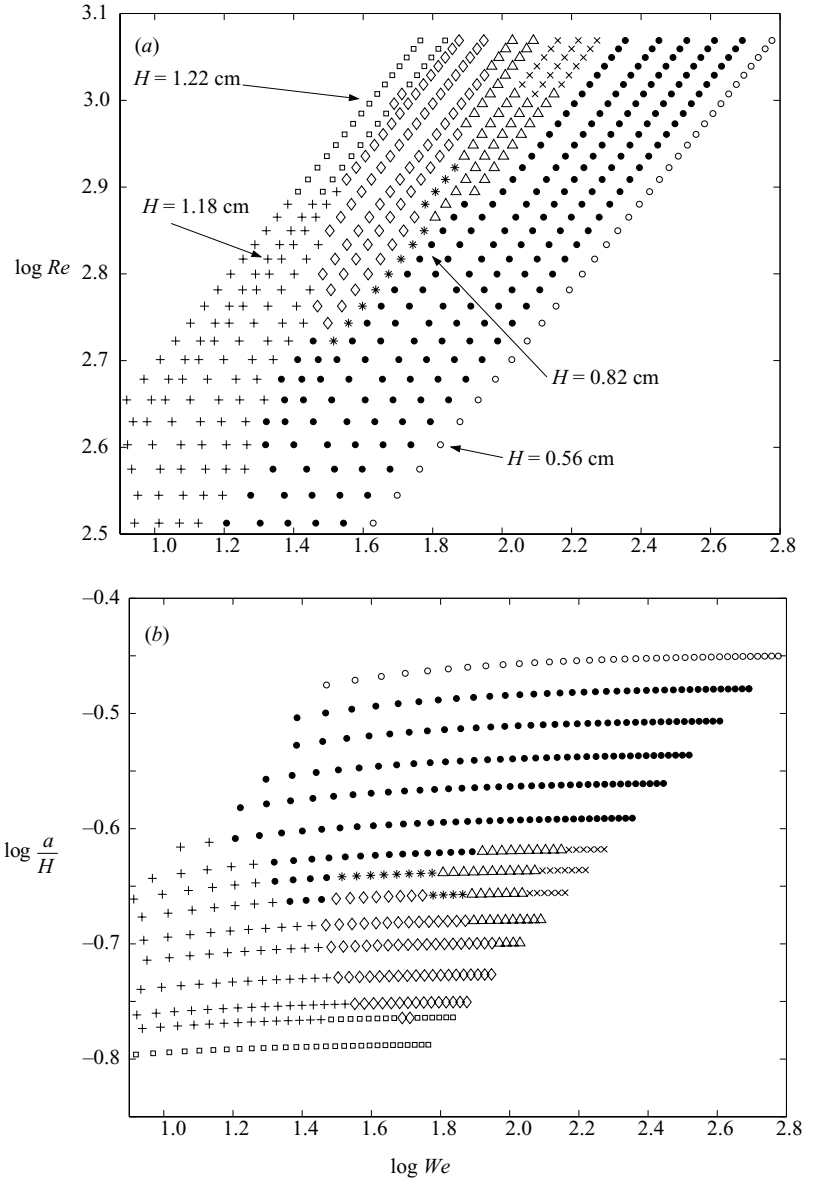

FIGURE 8. Two-dimensional projections of the surface of data obtained at $B = 0.74$ and presented in figure 9(c). All jumps were formed by a glycerine–water solution of viscosity 32 cS being released from a nozzle of radius 0.2 cm at a height 2.5 cm above the impact plate. (a) The dependence of the jump form on $Re = Qa/\nu$, and $We = \rho Q^2/(\sigma H^3)$. Different symbols denote the various jump shapes: △, three-leaf clover; ×, four-leaf clover; *, oval; ◇, bowtie; ○, Type I; ●, Type II; +, no jump. (b) The analogous dependence of jump structure on a/H and We.

clover-shaped jumps. This distinction is made in figures 7 and 8 for the data planes indicated, respectively, in figures 9(a) and 9(c). We note that the polygonal and clover jump regimes are both confined to limited regions of parameter space. Moreover, the polygonal jump regimes observed at $B = 6.53$ (figure 9d) in mineral oil, and by Ellegaard *et al.* (1998, 1999) in ethylene glycol are in adjacent regions of parameter

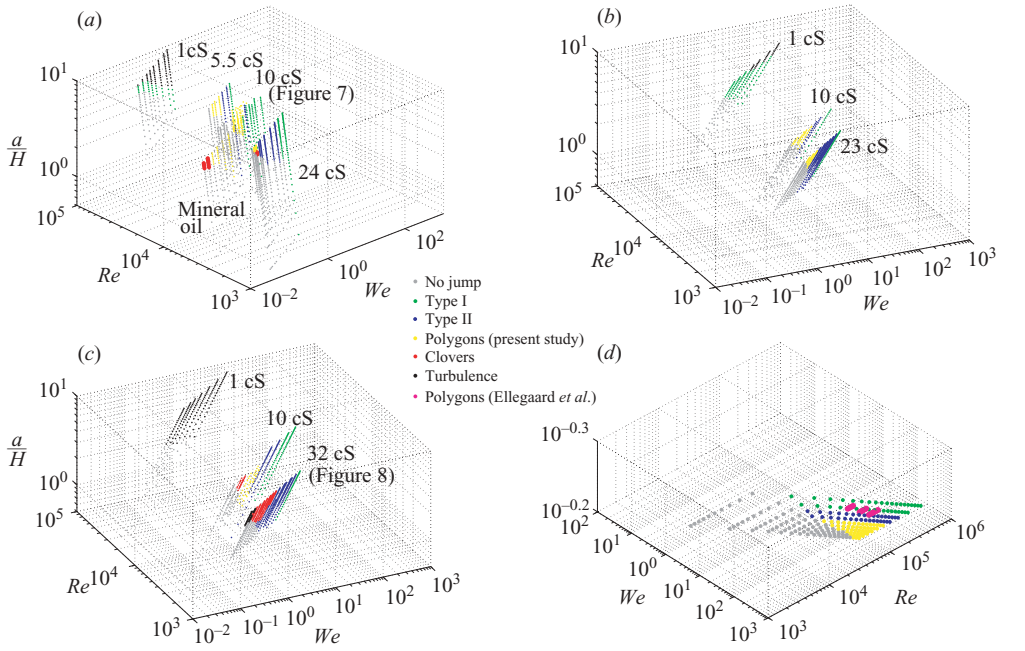

FIGURE 9. Regime diagrams indicating the dependence of the jump structure on the governing parameters $(We, Re, a/H)$ at fixed Bond numbers. (*a*) $B = 4.62$. Individual data planes correspond to fluids with viscosities indicated. The data plane at $\nu = 10\,\text{cS}$ is detailed in figure 7. Data were obtained with glycerol–water solutions with a nozzle radius of 0.5 cm. The mineral oil data were obtained with a nozzle of radius 0.38 cm, which allowed Bond number equivalence. (*b*) $B = 2.67$ corresponding to a nozzle radius of 0.35 cm. Individual data planes correspond to glycerol–water solutions with viscosities indicated. (*c*) $B = 0.74$ corresponding to a nozzle radius of 0.2 cm. Individual data planes correspond to glycerol-water solutions with viscosities indicated. The data plane at $\nu = 32\,\text{cS}$ is detailed in figure 8. (*d*) $B = 6.53$. The polygonal data of Elegaard *et al.* (1999), obtained with ethylene glycol, is presented in pink. The remaining data were obtained in our laboratory with mineral oil and a nozzle radius of 0.45 cm.

space. We note that the correspondence is not exact owing to the different properties of mineral oil and ethylene glycol: the surface representing Ellegaard *et al.*'s data is offset slightly relative to that obtained in our study.

We note that the jump structures were subject to strong hysteretic effects: the point of transition from one jump shape to another depended on whether the flow rate was increasing or decreasing. For each experiment, once the source parameters were established, we disrupted the jump structure by blowing on it; this initialization eliminated hysteresis from consideration.

5. Jump radius

Watson (1964) elucidated the dominant influence of viscosity on the circular hydraulic jump, and Bush & Aristoff (2003) calculated the relatively small correction to Watson's (1964) theoretical prediction for the jump radius required by consideration of surface tension. Viscosity results in vorticity diffusing from the lower boundary until spanning the fluid layer at a radial distance $r_v = 0.315 a Re^{1/3}$ from the point of

impact. For $r < r_v$, the surface speed is that of the incoming jet U, and the jump radius is defined by

$$\frac{R_j g H^2 a^2}{Q^2}\left(1+\frac{2}{B_j}\right)+\frac{a^2}{2\pi^2 R_j H}=0.10132-0.1297\left(\frac{R_j}{a}\right)^{3/2}Re^{-1/2}, \tag{5.1}$$

where $B_j = \rho g R_j \Delta H/\sigma$ is the jump Bond number and ΔH the height of the jump. For $r > r_v$, the surface speed is diminished relative to the incoming jet speed,

$$U(r)=\frac{27c^2}{8\pi^4}\frac{Q^2}{\nu(r^3+l^3)} \tag{5.2}$$

where $c = 1.402$ and $l = 0.567aRe^{1/3}$, and the jump radius is given by

$$\frac{R_j g H^2 a^2}{Q^2}\left(1+\frac{2}{B_j}\right)+\frac{a^2}{2\pi^2 R_j H}=0.01676\left[\left(\frac{R_j}{a}\right)^3 Re^{-1}+0.1826\right]^{-1}. \tag{5.3}$$

Finally, the layer depth in this outer regime ($r > r_v$) is given by

$$h(r)=\frac{2\pi^2}{3\sqrt{3}}\frac{\nu(r^3+l^3)}{Qr}. \tag{5.4}$$

We note that, owing to the influence of viscosity, the layer depth has a minimum at a critical radius that may be computed from (5.4).

Equations (5.1) and (5.3) were originally presented in Bush & Aristoff (2003) and differ from those of Watson (1964) only through inclusion of the $O(B_j^{-1})$ surface tension correction on the left-hand side. They rest on the same assumptions concerning the flow structure, specifically that the ratio of layer depths directly down- and upstream of the jump is large ($H/h \gg 1$), the flow is unidirectional in the thin film, and radial gradients in the hydrostatic pressure upstream of the jump are negligible relative to viscous stresses. Finally, Watson's prediction for jump radius rests on the assumption that the radial flow speed is constant beyond the jump, an assumption generally expected to be violated owing to separation beyond the jump, and to be least adequate for the Type II jumps. Watson's predictions for the circular jump radius were found by a number of investigators to be adequate for laminar jumps of large radius and depth, but to yield poor agreement in the opposite small-jump limit (Olson & Turkdogan 1966; Ishigai *et al.* 1977; Nakoryakov, Pokusaev & Troyan 1978; Bouhadepf 1978; Craik *et al.* 1981; Errico 1986; Vasista 1989; Liu & Lienhard 1993), where the surface tension correction becomes significant (Bush & Aristoff 2003). This small-jump regime is precisely that examined by Ellegaard *et al.* (1998, 1999) in which the polygonal jumps arise; consequently, we anticipate the relevance of this surface tension correction to our experimental study.

An experimental investigation of the dependence of the radii of strictly circular jumps on the governing parameters is presented in Bush & Aristoff (2003); here we focus our attention on the asymmetric jumps. The mean radius $\overline{R}_j$ of the asymmetric jumps was calculated from images by computing a suitable approximation to

$$\overline{R}_j=\frac{1}{2\pi}\int_0^{2\pi} r\,\mathrm{d}\theta. \tag{5.5}$$

For example, for polygons with number of sides $n > 6$, $\overline{R}_j$ was simply taken as the mean of the minimum and maximum jump radii. Figure 10 indicates the observed dependence of the mean jump radius $\overline{R}_j$. In order to facilitate comparison with

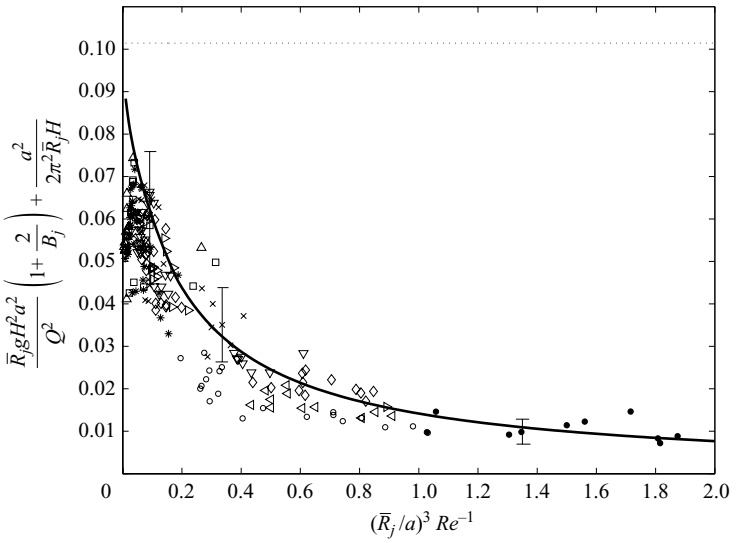

FIGURE 10. The dependence of the mean jump radius $\overline{R}_j$ on the governing parameters. The solid line represents the theoretical predictions (5.1) and (5.3). The dotted line represents the prediction of inviscid theory. Different symbols denote the various jump shapes: △, three-sided; □, four-sided; ∗, five-sided; ×, six-sided; ▽, seven-sided; ◇, eight-sided; ▷, nine-sided; ○, bowtie or butterfly; ◁, 3-leaf clover; ●, four-leaf clover. Characteristic error bars are shown.

equations (5.1) and (5.3), we plot the dependence of $(\overline{R}_j g H^2 a^2/Q^2)(1 + 2/B_j) + a^2/(2\pi^2 \overline{R}_j H)$ on $(\overline{R}_j/a)^3 Re^{-1}$. The dotted horizontal line indicates the inviscid theory, obtained from (5.1) in the limit of $Re \to \infty$, which is obviously inadequate in describing our data. The solid curve represents the jump radii predicted by (5.1) and (5.3). The mean radii of all steady structures observed, polygons and clovers, are reasonably well-described by the theoretical predictions.

We note that the discrepancy between theory and experiments for the mean jump radius is substantially larger than for the Type I circular jumps examined by Bush & Aristoff (2003). We expect this discrepancy to be a consequence of shortcomings in Watson's description of the flow in the regime examined here. While variance of the flow near the point of impact from purely radial violates the assumptions made in the development of equations (5.1) and (5.3), this did not introduce substantial errors in Bush & Aristoff's (2003) study of the Type I jumps. Moreover, the assumption that radial gradients in the hydrostatic pressure prior to the jump are negligible relative to viscous stresses is valid in the small-jump parameter regime examined in our study. We thus expect that the principal source of discrepancy between predicted and observed jump radii is the neglect of the influence of dynamic pressure downstream of the jump, an influence likely to be most pronounced in this regime (Bowles & Smith 1992; Higuera 1994; Yokoi & Xiao 2000, 2002). The principal source of measurement error arose from approximations made in calculating the mean jump radii of markedly asymmetric forms.

6. Jump stability

We propose a physical picture in which the instability of the initially circular jump is related to the Rayleigh–Plateau capillary pinch-off of a fluid thread. Plateau (1873) and Rayleigh (1879) demonstrated that a fluid thread bound by surface tension σ

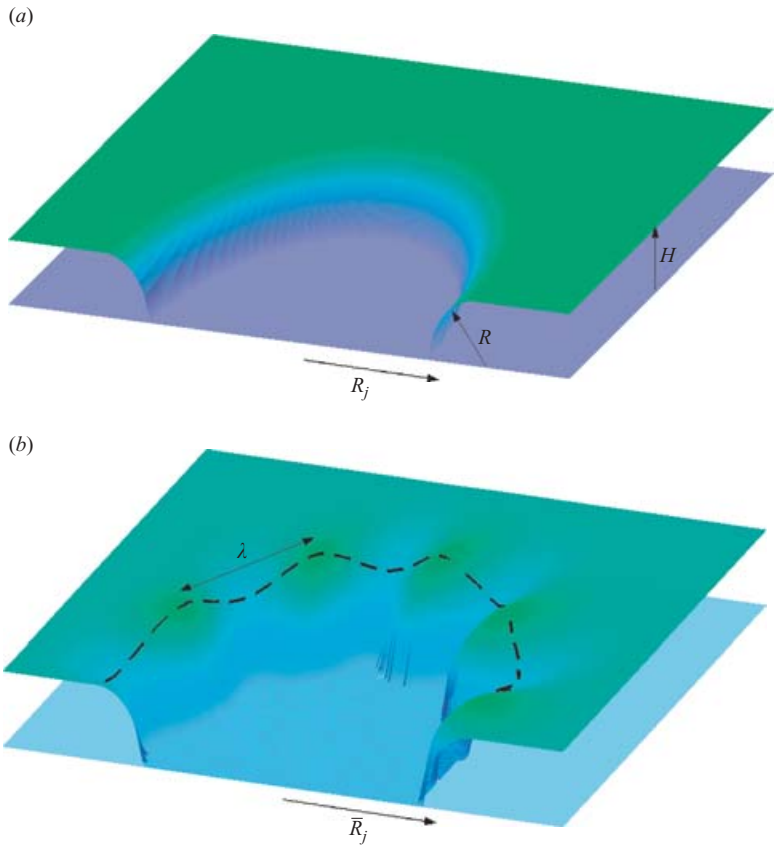

FIGURE 11. A schematic illustration of the capillary instability on a circular hydraulic jump, viewed as a portion of the inner surface of a torus. The unperturbed jump radius is R_j and R represents the radius of curvature of the jump in a vertical plane aligned with the mean flow. One expects a capillary instability to yield a wavelength of pinch-off, λ, proportional to R.

will become unstable to a varicose instability in order to minimize surface energy. The Ohnesorge number, $Oh = \sigma R/(\mu\nu)$, a Reynolds number based on the capillary wave speed σ/μ, prescribes the form of pinch-off of a fluid thread of radius R and dynamic viscosity $\mu = \rho\nu$ (Weber 1931; Chandrasekhar 1961). At high Oh, the pinch-off is resisted by fluid inertia, the time scale of instability is $(R^3\rho/\sigma)^{1/2}$, and the most unstable wavelength is $9.02R$. At low Oh, the pinch-off is resisted by fluid viscosity, the time scale of instability is $\mu R/\sigma$, and the most unstable wavelength increases with Oh. The jumps in our problem have characteristic height of $\Delta H \sim 0.2$–$1\,\mathrm{cm}$ and an Ohnesorge number of $O(100)$; consequently, the observed wavelengths of 0.7–2.0 cm are roughly consistent with the anticipated result of $4.51\Delta H$.

We propose a physical picture in which the jump is viewed as the inner portion of a torus whose axisymmetry is broken by a capillary instability (figure 11). In order to deduce the most unstable wavelength of instability, we must deduce the dominant curvature of the unperturbed circular jump. Since $R_j \gg \Delta H$, the curvature of the free surface in a vertical plane aligned with the mean flow necessarily dominates that associated with its azimuthal curvature: we thus need consider only the curvature in a vertical radial plane, $1/R$ (figure 11). The shape of the jump is determined by a balance between some combination of inertia, viscosity, gravity and surface tension. As in the

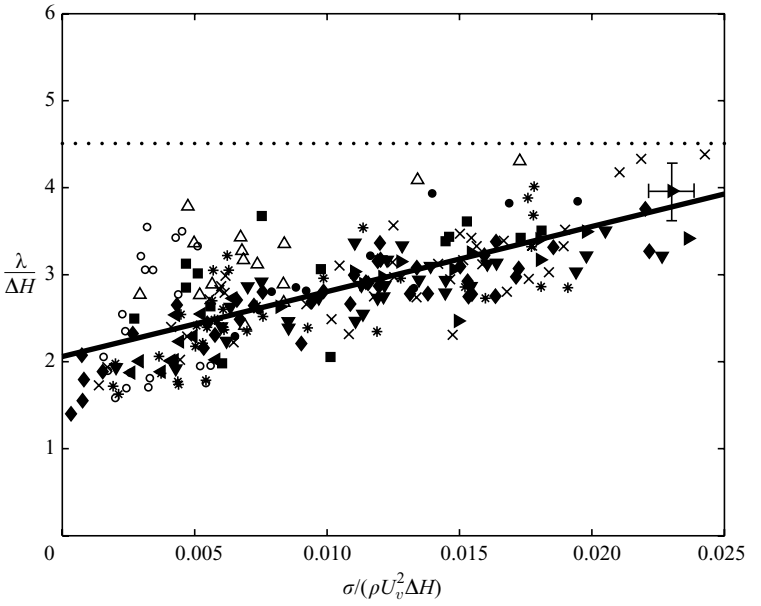

FIGURE 12. The observed dependence of the wavelength of instability on the governing parameters in the polygon and clover regimes. The wavelength is defined as the circumference of the jump divided by the number of sides: $\lambda = 2\pi \overline{R}_j / n$. Different symbols denote the various jump shapes: △, three-sided; □, four-sided; *, five-sided; ×, six-sided; ▽, seven-sided; ◇, eight-sided; ▷, nine-sided; ○, bowtie; ◁, 3-leaf clover; ●, four-leaf clover. Characteristic error bars are shown. The solid line represents the best-fit to the scaling (6.2). If the jump curvature is simply equal to its height ΔH, one expects the data to be described by the horizontal dotted line shown.

study of Ellegaard *et al.* (1998, 1999), asymmetric jumps only arose as an instability of the Type II circular jumps, that are adjoined by a toroidal vortex. In all experiments considered in our study, the characteristic vortex Reynolds number is large; for example, for a jump vortex with radius $R_v = 2\,\mathrm{mm}$ and flow speed $U_v = 30\,\mathrm{cm\,s^{-1}}$ in a fluid of viscosity 30 cS, the vortex Reynolds number is $Re_v = U_v R_v / \nu = 200$. One thus expects that the dominant curvature at the jump, $1/R$, will be set by a balance between surface tension and inertia:

$$\rho U_v^2 \sim \sigma / R. \tag{6.1}$$

U_v is the speed in the vortex adjoining the jump, taken to be the surface speed of the fluid layer at the base of the jump. For $\overline{R}_j < r_v$, this speed corresponds to that of the incoming jet $U_v = U$, while for $\overline{R}_j > r_v$, it is defined by (5.2) evaluated at the mean jump radius $\overline{R}_j$. The radius of curvature of the jump is thus prescribed by $R \sim \sigma/(\rho U_v^2)$. The theoretical description of the Rayleigh–Plateau instability indicates that the radius of curvature of the most unstable azimuthal mode has a wavelength proportional to R; therefore, we anticipate that

$$\lambda = C_1 \frac{\sigma}{\rho U_v^2}, \tag{6.2}$$

where C_1 is a coefficient to be determined.

Figure 12 indicates the observed dependence of the wavelength of instability of the jump on the governing flow parameters. All jump shapes observed in the polygon

and clover regimes are included. The wavelength is computed as $\lambda = 2\pi\overline{R}_j/n$, where n is the number of sides of the jump structure. Four-leaf clovers were taken as having eight sides, three-leaf clovers six, and bowties and butterflies four. For each data point, r_v was computed; either the incident jet speed U or (4.2) was assigned to U_v according to the relative magnitudes of r_v and $\overline{R}_j$. The data provide satisfactory agreement with (6.2); the best-fit line has a statistical correlation of 0.74. The constant of proportionality in (6.2) is thus deduced to be $C_1 = 74 \pm 7$. The line corresponding to $\lambda = 4.51\Delta H$, the result appropriate for the pinch-off of a stationary cylinder of diameter ΔH, is also plotted along with our data in figure 12. The mismatch supports our claim that the radius of curvature is not strictly proportional to ΔH but, rather, depends on the local dynamics.

It is noteworthy that the primary source of error in our prediction for the wavelength of instability results from the discrete number of sides; specifically, the mean circumference need not correspond to an integer multiple of the most unstable wavelength. The associated errors necessarily decrease as the number of sides increases; thus there is relatively large scatter in the data for bowtie and 3-sided jumps. Omission of these data increases the correlation coefficient from 0.74 to 0.8. Nevertheless, the scatter in the data apparent in figure 12 suggests that the jump instability is not the Rayleigh–Plateau instability in its purest form. The precise dynamical balance existing at the jump is complex, involving gravity, curvature, inertia and pressure (Bowles & Smith 1992; Higuera 1994; Yokoi & Xiao 2000, 2002; Watanabe *et al.* 2003). The principal shortcoming of our simple scaling argument is the relatively crude approximation made in deducing the dominant curvature of the jump, specifically that it may be obtained by balancing exclusively inertial and curvature forces.

7. Discussion

We have presented the results of an experimental investigation of the viscous hydraulic jump. In addition to the Type I, IIa and IIb circular jumps and the steady polygonal jump forms identified by previous investigators, we have identified a new class of steady asymmetric jumps that arise as an instability of the tiered Type IIb jumps, that we refer to as clovers (figure 4). Our exploration of parameter space (figures 7–9) has underscored the limited parameter regime in which both polygonal and clover jumps arise; this is presumably why none of these striking flow structures had been observed prior to the experiments of Ellegaard *et al.* (1998).

We note that the influence of fluid viscosity on the circular hydraulic jump is two-fold. First, viscosity acts to hasten the diffusion of vorticity across the fluid layer and so decelerate the flow. The concomitant decrease in the jump radius necessarily heightens the influence of surface tension on the jump. Second, viscosity acts to regularize the asymmetric frontal structure; this is, presumably, why the stable, steady polygonal or clover forms do not arise in water, where unsteady irregular frontal instabilities are the norm (Craik *et al.* 1981; Liu & Lienhard 1993).

Our study has clearly identified the importance of surface tension in prompting the axisymmetry-breaking instabilities observed in the circular hydraulic jump. While the significance of surface tension for jump stability was suggested by Craik *et al.* (1981) and Liu & Lienhard (1993), the mechanism for instability had not previously been considered. Ellegaard *et al.* (1998, 1999) suggest that the symmetry-breaking instability responsible for the polygonal jumps may be anticipated if one ascribes an effective line tension to the jump; however, they did not identify the origins of such a line tension with the surface tension. We here suggest that the instability may be

understood as being a manifestation of the Rayleigh–Plateau pinch-off of the initially circular jump, taken to be the inner section of a torus.

The addition of surfactant was observed to convert the polygonal jumps to circular jumps of relatively large mean radius. The associated reduction in surface tension results in expansion of the jump according to the theoretical developments of Bush & Aristoff (2003), and may result in the suppression of capillary pinch-off according to the present study. The influence of surfactant on the jump structure is complex, however, which is why a more quantitative study of the influence of surfactants was not undertaken. In particular, the surfactant acts to suppress motions marked by non-zero surface divergence such as those arising in the Type II jumps. The surfactant may thus have an impact on the jump structure not only through decreasing the surface tension, but also through suppressing the Type II planform that is a prerequisite for symmetry-breaking instability. The influence of surfactant on the stability of hydraulic jumps is left as a subject for future consideration.

Our experiments indicate that the mean jump radius is adequately described by the theory of Bush & Aristoff (2003), and that the wavelength of instability is given by (6.2) with $C_1 = (74 \pm 7)$. We note that these two results do not uniquely prescribe the jump shape in the nonlinear regime; for example, a six-sided jump could correspond to either a heptagon or a three-leaf clover. The non-axisymmetric jump shape may only be inferred from the source conditions by reference to our regime diagrams (figures 7–9). We do not expect that the complex dynamical balance arising at the jump can be captured satisfactorily with a simple scaling: the shortcomings of the scaling are evident in the scatter of the data. For example, one expects the downstream flow, specifically the dynamic pressure associated with the jump vortex, to have a significant influence on the pinch-off at the jump. Nevertheless, the scaling does capture some of the dominant physics; this is why, presumably, it yields a reasonable collapse of the data.

One key observation made originally by Ellegaard *et al.* (1998, 1999) and again in our study is that the asymmetric forms only emerge from the Type II jumps. This we ascribe to one of two physical effects. First, the importance of surface tension will be most pronounced for jumps with large surface area and heightened curvature; one expects the curvature of the interface to be most pronounced for Type II jumps owing to the influence of the eddies adjoining the jump. Second, the presence of the vortex will tend to destabilize the jump owing to the influence of the radial centripetal force; the analogous destabilizing influence of rotation in the Rayleigh–Plateau problem has been demonstrated by Hocking & Michael (1959), Hocking (1960) and Pedley (1967).

We note that many of the observed jumps are marked by sharp cusps in their corners (e.g. figure 3*a*, *b*) as frequently arise in convergent flows dominated by viscosity and surface tension, for example, in the four-roll mill (Joseph *et al.* 1991). Surface tension typically serves to regularize the corner flows unless the flows are sufficiently vigorous to prompt air entrainment at the cusp (Eggers 2000). Our observations indicate that entrainment of air may arise at both the base of the jump and at the corners of the polygonal jumps. While we have proposed capillary pinch-off as the source of the symmetry-breaking instabilities in the hydraulic jump, the detailed calculation of jump shapes is left as a subject for future investigation.

While the capillary instability is best known as the source of pinch-off of a cylindrical fluid thread (Plateau 1873; Rayleigh 1879), it prompts analogous instabilities in a variety of geometries; for example, in liquid menisci bound at solid edges (Langbein 1990). Figure 13 illustrates a number of free-surface flows in which symmetry-breaking is prompted by a capillary instability. The capillary pinch-off of the toroidal rim on

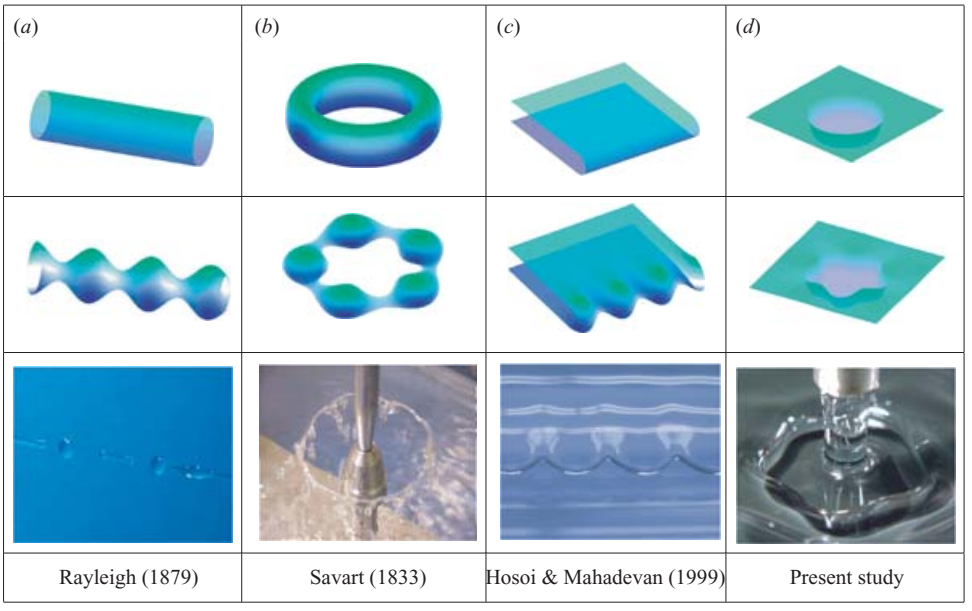

FIGURE 13. Symmetry-breaking forced by capillary instabilities. (*a*) The classic Rayleigh–Plateau instability prompts the pinch-off of a cylindrical fluid thread into a series of drops. (*b*) Capillary instability of the toroidal rim on a radially expanding circular fluid sheet releases discrete droplets from the sheet edge. (*c*) Capillary instability on the advancing front within a partially filled cylinder rotating about its horizontal axis. (*d*) The transformation of the circular jump into asymmetric forms.

a radially expanding circular fluid sheet (Savart 1833) leads to the release of discrete droplets at the sheet edge. The hydraulic jump instability bears a resemblance to that arising when a partially filled cylinder is rotated about its horizontal axis of symmetry (Karweit & Corrsin 1975; Thoroddsen & Mahadevan 1997; Hosoi & Mahadevan 1999, shown in figure 13*c*). The frontal instability so observed is likewise caused by a capillary instability of a curved fluid front; however, in their flow, the characteristic Reynolds number is small. The dominant force balance at the front is thus between viscous stresses and capillary forces, consideration of which yields a most unstable wavelength that scales as $H(\mu U/\sigma)^{-1/3}$ where U is the speed of the cylinder wall and H is the fluid depth. By contrast, the hydraulic jump considered here is characterized by a high Re: the curvature of the jump and the concomitant wavelength of azimuthal instability are prescribed by a balance between curvature and inertial forces. Nevertheless, both systems are marked by vortical motions steepening fronts and so promoting capillary instability.

While the majority of the observed shapes could be classified as belonging in either circular or polygon or clover or turbulent regimes, there are a number of exceptions and oddities. First, there is an unsteady flow regime between the polygon and fully turbulent regimes in which the roller vortex adjoining the jump lifts off, resulting in an apparent crown on the jump (figure 14). Second, situations arose where the outer layer was too deep to support a hydraulic jump, but where a roller vortex was observed to form. In certain parameter regimes, this vortex became unstable and assumed a roughly polygonal shape. Such an instability is clearly not a manifestation of capillary pinch-off, but may be related to the instability mechanism responsible

FIGURE 14. The crown-shaped jump arising in a glycerol-water solution of viscosity 5 cS, an intermediary between the polygonal and fully turbulent regimes.

for the break-up of a circular smoke ring into polygons (Widnall & Tsai 1977). Such oddities are left as problems for future consideration.

The authors thank Tomas Bohr for valuable discussions, Gareth McKinley and José Bico for granting us access to their surface tensiometer, and Jeff Leblanc for his assistance with the experimental study. The authors gratefully acknowledge the financial support of the National Science Foundation through Career Grant CTS-0130465 (J.W.M.B.) and Grant DMS-0243591 (A.E.H.).

REFERENCES

BERGTHORSSON, J., SONE, K., MATTNER, T., DIMOTAKIS, P., GOODWIN, D. & MEIRON, D. 2005 Experiments and modeling of impinging laminar jets at moderate separation distances. *GALCIT Rep.* **3**, 1–25.

BOHR, T., DIMON, P. & PUTKARADZE, V. 1993 Shallow-water approach to the circular hydraulic jump. *J. Fluid Mech.* **254**, 635–648.

BOHR, T., PUTKARADZE, V. & WATANABE, S. 1997 Averaging theory for the structure of hydraulic jumps and separation in laminar free-surface flows. *Phys. Rev. Lett.* **79**, 1038–1042.

BOUHADEPF, P. 1978 Etalement en couche mince d'un jet liquide cylindrique vertical sur un plan horizontal. *Z. Angew. Math. Phys.* **29**, 157–167.

BOWLES, R. & SMITH, F. 1992 The standing hydraulic jump: Theory, computations and comparisons with experiments. *J. Fluid Mech.* **242**, 145–168.

BUSH, J. & ARISTOFF, J. 2003 The influence of surface tension on the circular hydraulic jump. *J. Fluid Mech.* **489**, 229–238.

CHANDRASEKHAR, S. 1961 *Hydrodynamic and Hydromagnetic Stability*. Dover.

CRAIK, A., LATHAM, R., FAWKES, M. & GIBBON, P. 1981 The circular hydraulic jump. *J. Fluid Mech.* **112**, 347–362.

EGGERS, J. 2000 Air entrainment through free-surface cusps. *Phys. Rev. Lett.* **86**, 4290–4293.

ELLEGAARD, C., HANSEN, A., HAANING, A., HANSEN, K. & BOHR, T. 1996 Experimental results on flow separation and transitions in the circular hydraulic jump. *Physica Scripta* **T67**, 105–110.

ELLEGAARD, C., HANSEN, A., HAANING, A., HANSEN, K., MARCUSSON, A., BOHR, T., HANSEN, J. & WATANABE, S. 1999 Polygonal hydraulic jumps. *Nonlinearity* **12**, 1–7.

ELLEGAARD, C., HANSEN, A., HAANING, A., MARCUSSON, A., BOHR, T., HANSEN, T. & WATANABE, S. 1998 Creating corners in kitchen sink flows. *Nature* **392**, 767–768.

ERRICO, M. 1986 A study of the interaction of liquid jets with solid surfaces. PhD Thesis, University of California San Diego.

Higuera, F. 1994 The hydraulic jump in a viscous laminar flow. *J. Fluid Mech.* **274**, 69–92.

Higuera, F. 1997 The circular hydraulic jump. *Phys. Fluids* **9**, 1476–1478.

Hocking, L. 1960 The stability of a rigidly rotating column of liquid. *Mathematika* **13**, 1–9.

Hocking, L. & Michael, D. 1959 The stability of a column of rotating liquid. *Mathematika* **6**, 25–32.

Hosoi, A. & Mahadevan, L. 1999 Axial instability of a free-surface front in a partially filled horizontal cylinder. *Phys. Fluids* **11**, 97–106.

Ishigai, S., Nakanishi, S., Mizuno, M. & Imamura, T. 1977 Heat transfer of the impinging round water jet in the interference zone of film flow along the wall. *Bull. JSME* **20**, 85–92.

Joseph, D., Nelson, J., Renardy, M. & Renardy, Y. 1991 Two-dimensional cusped interfaces. *J. Fluid Mech.* **223**, 383–409.

Karweit, M. & Corrsin, S. 1975 Observation of cellular patterns in a partly filled, horizontal, rotating cylinder. *Phys. Fluids* **18**, 111–112.

Langbein, D. 1990 The shape and stability of liquid menisci at solid edges. *J. Fluid Mech.* **213**, 383–409.

Liu, X. & Lienhard, J. 1993 The hydraulic jump in circular jet impingement and in other thin liquid films. *Exps. Fluids* **15**, 108–116.

McCarthy, M. & Malloy, N. 1974 Review of stability of liquid jets and the influence of nozzle design. *Chem. Engng J.* **7**, 1–20.

Nakoryakov, V., Pokusaev, B. & Troyan, E. 1978 Impingement of an axisymmetric liquid jet on a barrier. *Intl J. Heat Mass Trans.* **21**, 1175–1184.

Olson, R. & Turkdogan, E. 1966 Radial spread of a liquid stream on a horizontal plate. *Nature* **211**, 813–816.

Pedley, T. 1967 The stability of rotating flows with a free surface. *J. Fluid Mech.* **30**, 127–147.

Plateau, J. 1873 *Statique Experimentale et Théorique des Liquides Soumis aux Seules Forces Moleculaires*. Paris: Gauthier-Villars.

Rayleigh, Lord 1879 On the capillary phenomena of jets. *Proc. R. Soc. Lond.* A **29**, 71–97.

Rayleigh, Lord 1914 On the theory of long waves and bores. *Proc. R. Soc. Lond.* A **90**, 324.

Savart, F. 1833 Mémoire sur le choc d'une veine de liquide lancé contre un plan circulaire. *Ann. Chim. Phys.* **59**, 113–145.

Tani, I. 1949 Water jump in the boundary layer. *J. Phys. Soc. Japan* **4**, 212–215.

Thoroddsen, S. & Mahadevan, L. 1997 Experimental study of coating flows in a partially-filled horizontally rotating cylinder. *Exps. Fluids* **23**, 1–13.

Vasista, V. 1989 Experimental study of the hydrodynamics of an impinging liquid jet. B. Eng. Thesis, MIT.

Watanabe, S., Putkaradze, V. & Bohr, T. 2003 Integral methods for shallow free-surface flows with separation. *J. Fluid Mech.* **480**, 233–265.

Watson, E. 1964 The spread of a liquid jet over a horizontal plane. *J. Fluid Mech.* **20**, 481–499.

Weber, C. 1931 Zum zerfall eines flussigkeitsstrahles. *Z. Angew. Math. Mech.* **462**, 341–363.

Widnall, S. & Tsai, C.-Y. 1977 The instability of the thin vortex ring of constant vorticity. *Proc. R. Soc. Lond.* A **287**, 273–305.

Yokoi, K. & Xiao, F. 2000 Relationships between a roller and a dynamic pressure distribution in circular hydraulic jumps. *Phys. Rev.* D **61**, 1016–1019.

Yokoi, K. & Xiao, F. 2002 Mechanism of structure formation in circular hydraulic jumps: Numerical studies of strongly deformed free-surface shallow flows. *Physica* D **161**, 202–219.